PAPER

Time-resolved ion energy distribution functions during a HiPIMS discharge with cathode voltage reversal

Physica Scripta

PAPER

Time-resolved ion energy distribution functions during a HiPIMS discharge with cathode voltage reversal

RECEIVED
3 October 2022

REVISED
17 November 2022

ACCEPTED FOR PUBLICATION
24 November 2022

PUBLISHED
6 December 2022

Zachary Jeckell[1,*], **David E Barlaz**[1], **Thomas Houlahan**[2], **Wolfgang Huber**[2], **Ian Haehnlein**[2], **Brian Jurczyk**[2] **and David N Ruzic**[1]

[1] Department of Nuclear, Radiological, and Plasma Engineering, University of Illinois at Urbana-Champaign, Urbana, IL, United States of America
[2] Starfire Industries, Champaign, IL, United States of America
[*] Author to whom any correspondence should be addressed.

E-mail: druzic@illinois.edu

Keywords: HIPIMS, cathode reversal, ion energy distribution, sputtering, PVD

Abstract

The effect on the ion energy distribution function (IEDF) of plasma produced during a high-power impulse magnetron sputtering (HiPIMS) discharge as the pulse conditions are varied is reported. Pressure was varied from 0.67–2.00 Pa (5–15 mTorr), positive kick pulses up to 200 V tested with a constant 4 μs delay between negative and positive cycles. The results demonstrate that the resulting plasma during the positive cathode voltage reversal is the result of expansion through the largely neutral gas species between the end of the magnetic trap of the target and the workpiece. The plasma potential rises on similar time scale with the evolution of a narrow peak in the IEDF close to the applied bias. The peak of the distribution function remains narrow close to the applied bias irrespective of pulse length, and with only slight pressure dependence. One exception discovered is that the IEDF contains a broad high energy tail early in the kick pulse due to acceleration of ions present beyond the trap from the main pulse separate from the ionization front that follows.

1. Introduction

Crucial to the adoption of high-power impulse magnetron sputtering (HiPIMS) as both a research and production deposition technique is the improvement in deposition rate [1–3], relative to direct current magnetron sputtering (dcMS) [4]. Previous efforts have included alterations to magnet pack design [5–7], and shortening of the negative pulse length [8,9]. Substantial effort was made to experimentally demonstrate the ability of HiPIMS to generate increased ion fraction [10] through manipulation of the negative pulse alone [11,12], typically at pressures below 1.33 Pa. This has paralleled both modelling and experimental efforts to gain an improved understanding of the role of self-sputtering and ion return to the cathode [7,13–16] and built on earlier work measuring the ion fraction and ion energy distribution in ionized PVD systems [17,18]. More recently, addition of a positive pulse[3] to the discharge series as a means of releasing ionized material from the magnetic trap has been proposed for many years [19,20], and was first commercialized in the past five years [19,21]. Details of the discharge as discussed elsewhere [21]; the advantage of the positive cathode voltage reversal, or 'kick' pulse is that following a negative bias 'main' pulse, a kick pulse with user controlled amplitude and duration is applied to the magnetron cathode after a user defined delay. The effect of the kick pulse being increased ion fraction [22], deposition rate [19], as well as tuneable ion energy [1] of the deposited material.

In addition to increasing deposition rate, the positive pulse allows one to control the ion energy reaching the substrate. Since changes to electric field are felt by ionized sputtered material and process gas alike, the need to understand and to separate the effects of metal and gas ions has arisen [22–24]. The importance of tuneable ion energies of deposited material are difficult to understate given the wide range of material properties [25]

3 HiPIMS utilizing a positive pulse has been referred to as both a 'kick' pulse as well as 'bipolar' HiPIMS in literature. This article uses the kick term to avoid overlap with the use of bipolar to refer to pulsed substrate biasing, anode biasing, etc.

accessible at relatively modest gas temperatures. In addition to improved adhesion of metal [26] and nitride [27,28] films, as well as other traditional applications for physical vapor deposition (PVD), HiPIMS with controllable ion energies could circumvent the scalability challenges of higher energy deposition techniques such as pulsed laser deposition (PLD) or molecular beam epitaxy (MBE).

Concurrently, the mechanism by which ionized material reaches the substrate has become a matter of keen interest. One proposed mechanism is that the raising of plasma potential (V_p) at the target surface provides a sufficient electric field for ionized material to escape the magnetic trap of the magnetron with acceleration across a magnetic field gradient reminiscent of a Hall Thruster. Ionization of neutrals occurs with plasma expansion, though acceleration of existing ions dominates. This argument has been supported by V_p measurements near the magnetron surface [26], and at grounded substrates [29] in which V_p rises with the beginning of the pulse, but falls off rapidly axially from the target. A second mechanism is that the raised plasma potential commutes across the magnetic trap and V_p is raised uniformly throughout the chamber. In such a discharge, in addition to metal ions being released from the target, neutral metal atoms could also be ionized by the expanding plasma volume and dominate the ion flux. The hypothesis for V_p commuting is demonstrated by examining the time resolved EEDF which show fast electrons at the start of the positive pulse [23], which is also believed to have a higher chance of causing enroute ionization [23]. Given the significant mobility differences between ions and electrons, such a mechanism should be visible in transit times for V_p and floating potential (V_f) varying with chamber conditions such as pressure.

There is also some concern given the possibility of different mechanisms dominating depending on combinations of chamber geometry, magnet pack configuration, and other parameters that will be specific to the user. For example, in one of the early measurements of current at the cathode in a HiPIMS discharge with a positive pulse the current waveform is a strong function of delay between negative and positive pulse [30]; this was explained on the basis of electrons diffusing slowly away from magnetic trap. In a follow-up paper, the same group observed two waves of current both at the cathode as well as a grounded probe [31]. At the cathode the waves are attributed to residual electrons in the sheath followed by electrons in the magnetic trap; the probe from a nearby ion population similar to the pseudo-Hall thruster mechanism above followed by thermalized ions. Both papers utilize a balanced magnet pack and report strong pressure dependence to their observations indicating that the magnetic trap is limiting plasma expansion during the positive pulse. This suggests that a sheath is not formed quickly at the grounded probe or other workpiece, limiting ion acceleration.

Concurrently, there was a significant effort to better resolve the effects of both main [11] and kick pulse on gas to metal ion ratios using mass spectrometer based techniques [1,22,24,32] with a wide variety to main to kick delays times. Unlike the ion current measurements, these experiments utilized an unbalanced magnet pack in the magnetron and the differences were apparent. Significant populations of both metal and gas species were observed near the applied kick bias (single ionized) and at double the energy (doubly ionized). These works did not vary pressure, however the uniformity of ion energy strongly suggests the formation of a sheath at the probe surface due to the plasma expansion mechanism discussed above and supported by floating potential [29] and Langmuir probe measurements [33].

In this paper, we report time-resolved ion energy distribution function (IEDF) measurements for a HiPIMS discharge utilizing the Starfire Industries 2-2 IMPULSE® with Positive Kick™ with a kick pulse of user defined delay, bias amplitude, and duration. The transient events are systematically studied across a wide range of operating conditions including pressure, kick pulse amplitude and length while holding the main to kick delay at a constant 4 μs. Ion energy distributions, and floating potential measurements, during the rise, hold, and decay periods of the kick pulse will be used to support the argument that at the pressures used here (0.67 to 2.00 Pa) plasma potential transits the entire chamber and ionized material arriving at the substrate is ionized by the expanding plasma to a significant degree with the exception of the first few μs of the kick pulse. There is some evidence that at lower pressures and short pulse lengths the pseudo-Hall Thruster type mechanism gains in importance.

2. Experimental details

All experiments were performed in a high vacuum chamber with a base pressure that ranged from $\sim 10^{-5}$ to $\sim 10^{-3}$ Pa depending on pumping conditions. The chamber was equipped with 4″ unbalanced TORUS magnetron from Kurt J Lesker Co. containing a ¼″ Zr target (Lesker, Grade 702). The magnetron was powered by a Starfire Industries 2-2 IMPULSE® with Positive Kick™ backed by a MagnaPower XR Series 2 kV, 1 A direct current supply. Operating pressure was read from a capacitance manometer, base pressure from an ion gauge, Ar (Airgas UHP) was delivered via a mass flow controller.

Between the Impulse output and the magnetron was a shielded metal box through which the centre conductor passed through a Pearson 410 coil attached to high voltage probes. The magnetic induction current in

Figure 1. Displacement current abatement for Semion probe body. Probe body (left) was encased using polyimide tape (centre) followed by aluminium foil (right). The foil was grounded to chamber body to shunt displacement current while the probe body is grounded only through probe electrical connections. Blue arrows mark the active area openings.

Table 1. Magnetron discharge conditions used throughout the study. Frequency was typically adjusted to ensure stable discharge. There was a 4 μs delay between the end of the main pulse and the positive cathode reversal.

	Main pulse		Positive cathode reversal		
Pressure	Voltage	Width	Voltage	Width	Frequency
Pa	V	μs	V	μs	Hz
0.67–2.00	−600–−800	15–150	0–200	0–100	250–500

the coil served as a more accurate measurement of current delivered to the magnetron than the output displayed by the Impulse's internal measurement system. The measured impedance of both the measurement circuit and the coaxial cables from the Impulse to the magnetron were less than 1 μH. The internal synchronization signal of the Impulse was used to trigger both the gridded energy analyser as well as the oscilloscope collecting the HiPIMS waveform from the Pearson coil and probes. The oscilloscope also collected a reading of V_f from a bare wire floating probe made from a partially stripped coaxial cable.

Measurements of IEDF were acquired using a Impedans Semion Retarding Field Energy Analyzer (RFEA). Button probes with 7 holes (10 μA current setting) were used to maximize sensitivity to small current. Probe to target distance was held fixed at 8 cm. Initially, the probe body collected significant displacement current near the beginning of the kick pulses, despite being grounded to the chamber walls. It was determined that the displacement current was due to parasitic capacitance between the probe body and collection grids being too large. Under these conditions, time resolution lost for >5 μs by which time V_f had already undergone significant rise. To prevent such large displacement currents, the probe body was insulated from the chamber body and placed inside a metal box with an aperture approximately the size of the active area encompassing the 7 holes as shown in figure 1. With the metal box grounded to the chamber body, displacement currents during transitions in V_p were no longer observed as the metal box formed a second smaller parasitic capacitor in series. This allowed for temporal resolution of 1 μs or less to be achieved throughout the study.

Energy detection ranges in the Semion software were selected to ensure detection at ∼30% higher than expected peak ion energies (75–150 eV depending on kick pulse bias). Energy resolution was considered to be ∼1% of the energy range, i.e.: 1 eV for a 100 eV full range. Individual as well as averaged scans were acquired in order to observe discharge instabilities. As stable operating conditions were achieved, scan averaging was increased to 16 scans to assist in electronic noise filtering. Additionally, there are two other delays known as first step delay and step delay. The first step delay is the delay between scans, and the step delay is the delay in time between changing voltage and a new acquisition. For time-resolved measurements these delays need to be roughly 100 times higher than for time averaged measurement. For this work a first step delay of 1 s and a step delay of 40 ms were used. The integration ('ADC' software setting) was set to 4,000 measurements for each data point for this work.

Discharge conditions were selected based on regimes of stable magnetron operation in order to maximize the range of observable conditions. A list of variables of concern and their settings or ranges tested can be seen in table 1. In general, frequency was varied independently of variables being tested to ensure stability; 250 Hz was sufficient for all conditions except the shortest main pulses. The voltage of the main pulse was adjusted independently for each test based on a desire to perform all tests in a self-sputtering/gas rarefaction mode [34]. Rarefaction was achieved when the HiPIMS current waveform reached a flat line towards the end of the pulse rather than either dropping due to exhausting ionizable gas near the magnetron or climbing due to runaway self-sputtering of metal ions. This was done to ensure the highest concentration of metal ions. An example HiPIMS

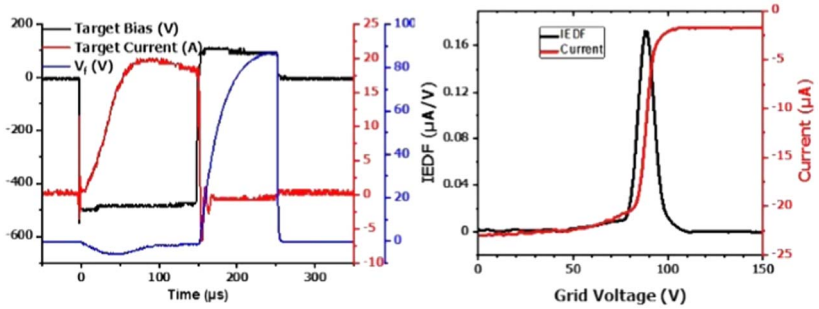

Figure 2. Left: HiPIMS waveform collected over the duration of the pulse with floating potential from probe overlaid at a pressure of 2.00 Pa, a main pulse width of 150 μs, a kick width of 100 μs at a positive target kick voltage of 100 V. Right: Semion software output 50 μs into a 100 V kick pulse. Collected current is near zero below a retarding potential of ~90 V and rises over the width of the ion energy peak. The baseline ion energy possesses a degree of noise, though kick pulse peaks are clearly distinguished.

waveform trace can be seen in figure 2. Additionally, the peak to peak voltage difference between the main and kick pulses were limited to 1200 V to protect against hardware damage. Current density was confirmed to always be below the threshold for spoke or hot spot formation [3,35]. Based on observations of low populations of multiple ionization events (based of RFEA signal), the applied bias (V) corresponds to the ion energy (eV) for purposes of discussing IEDF results.

3. Results and discussion

The Impedans Semion software saves the IEDF as well as ion current. A representative example of the software output is shown in figure 2. Individual IEDF traces at known times may then be combined into a waterfall plot, such as that seen in figure 3 for better visualization of changes to the IEDF throughout the HiPIMS pulse for three different pressures. While the population of single ionized species is clearly visible in the distribution function, the RFEA did not possess sufficient sensitivity to observe populations of double or higher ionization species as seen in other literature utilizing mass spectrometer based detection [1,22]. The corresponding current and voltage waveforms for the discharges are compiled in figure 4 along with the IEDF at select time slices to better show the evolution of the IEDF as well as directly compare across pressure.

A variety of parameters were then extracted from these plots in order to better compare discharge behaviour across the conditions tested. Extracted parameters included the total ion current and the energy of peak intensity in the IEDF. Calculated parameters include the transit time of the plasma to the probe, as well as the width of the energy distribution as a function of time.

3.1. Transit time

Transit time was defined as the time from the start of the kick pulse for the voltage of the maximum intensity peak of the IEDF to reach 67% of the applied kick pulse voltage as illustrated in figure 5. Due to resistive loses in the cable as well as the plasma, the maximum energy index never reaches kick voltage regardless of conditions tested. The applied kick voltage was nonetheless selected as a reference point to ensure that any differences between final voltage of maximum energy and applied kick voltage that varied with discharge conditions did not obscure differences in transit times.

Despite the variation in operating pressure, the mean free path (MFP) for Ar at 300 K remains <1 cm throughout the study ensuring that collisions between ions/electrons and the neutral gas occur between the magnetron and probe. Given a collisional regime, one might expect the transit time of the plasma to vary with MFP. Instead, the transit time was found to be consistently between 2–4 μs regardless of pressure or other conditions. This implies that the electric field variation transits to the substrate faster than the ions themselves, similar to the propagation of an ionization front of plasma bullets [36,37]. In this case, it is not an ionization front that moves from the target to the substrate, but rather fast electrons This is consistent with measured floating potential and V_p rise times in the literature [24,32] and direct measurements of the time-resolved electron energy distribution functions shown in a companion paper [33]. In the literature it is reported that the plasma and floating potential are capable of commuting distances of 100 mm in as little as a few microseconds [24], which supports the argument that the increase in energy of ions reaching the substrate is due to increase in potential rather than diffusion of ions which can take on the order of 10's of microseconds [38]. Our measured floating potential does not appear to commute as fast, but this could be due to chamber geometry, or location

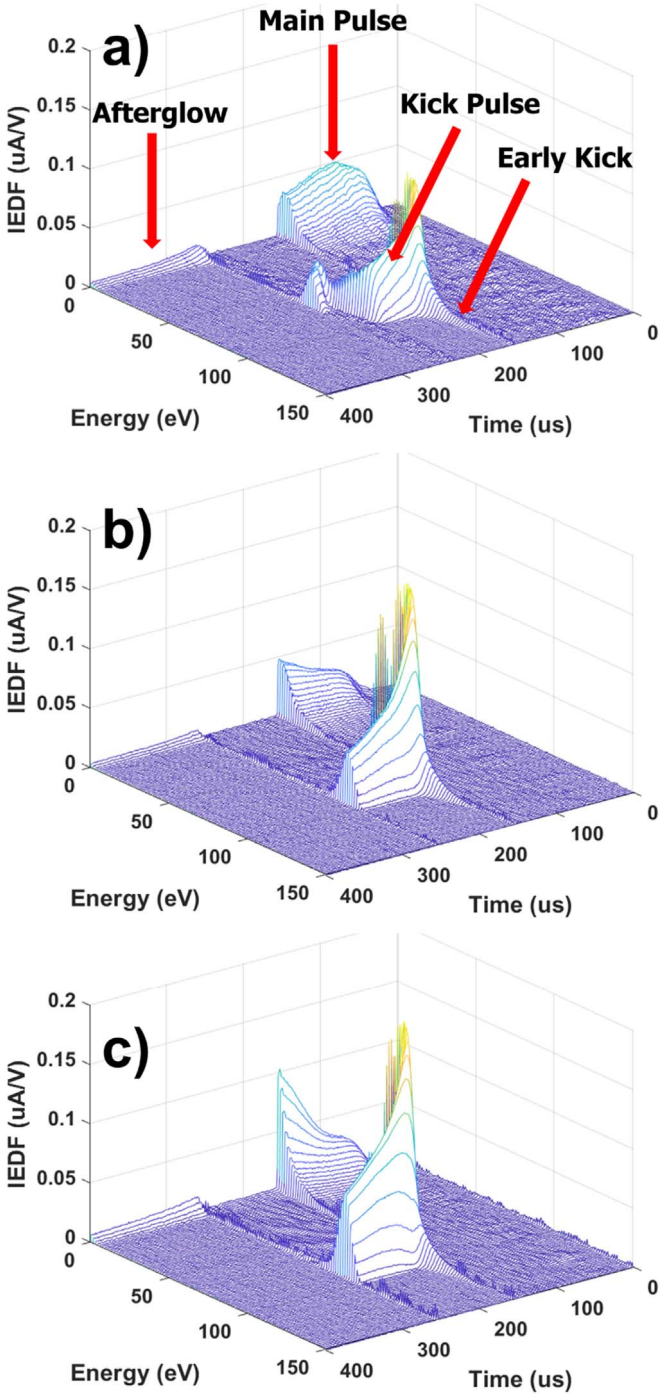

Figure 3. Waterfall plot encompassing a full HiPIMS discharge. Conditions: (a) 0.67 Pa, (b) 1.33 Pa, (c) 2.00 Pa, 150 μs main pulse, 100 μs kick pulse, 100 V positive target voltage. Annotations of discharge regions on the top panel reflect nomenclature used throughout this work.

near a grounded surface. At the probe surface the sheath is collisionless as would be expected for the pressure range tested and is consistent with other observations [22].

3.2. Peak ion energy

As mentioned above, the centre of the IEDF never reaches the applied kick voltage due to resistive loses. While this may be accounted for at the level of materials processing applications by tuning the kick voltage based on a desired energy distribution at the workpiece, determining what processing parameters strongly affect this offset is desirable. As is seen in figures 2 and 4 but shown more clearly in figure 6, pressure does have a small effect on the peak ion energy, and how quickly that peak is obtained. Higher pressure slightly lowers the ion energy maximum and delays when that maximum is reached. This is due to collisions of the electrons and ions with the neutral gas delaying the diffusion rate of the maximum potential commuting to the substrate. Direct

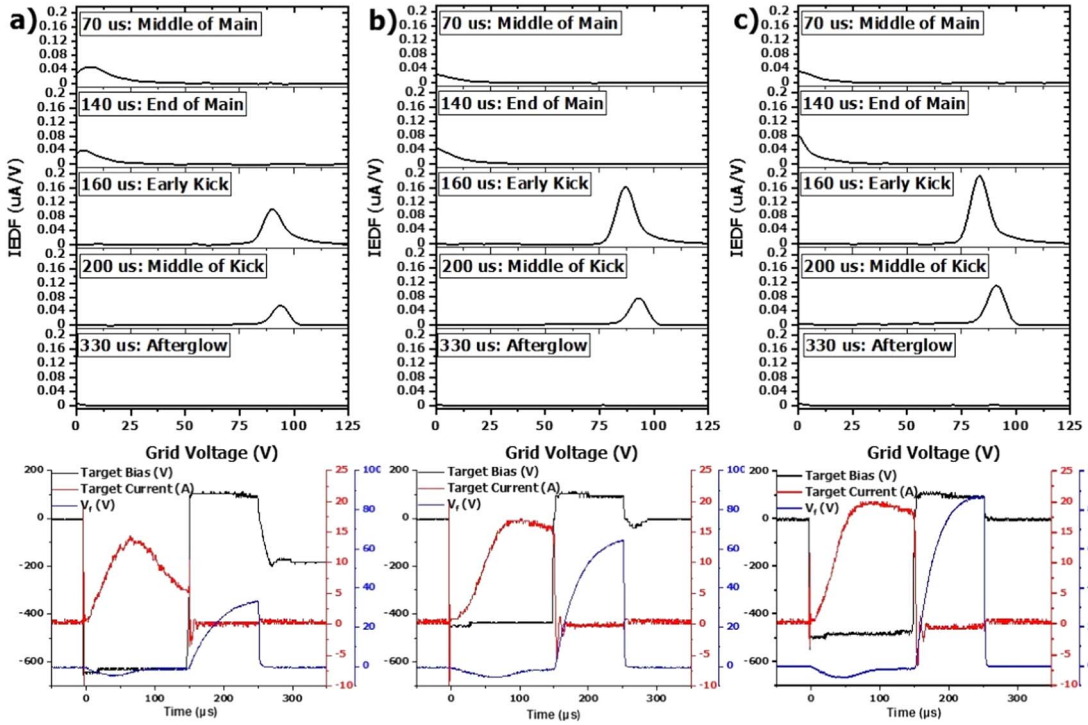

Figure 4. Top: IEDF slices showing different portions of the discharge at (a) 0.67 Pa, (b) 1.33 Pa, and (c) 2.00 Pa. Bottom: Corresponding IV waveforms collected from the magnetron sensors. Conditions: 150 μs main pulse, 100 μs kick pulse, 100 V positive target voltage, with main pulse negative bias varied to retain rarefaction state.

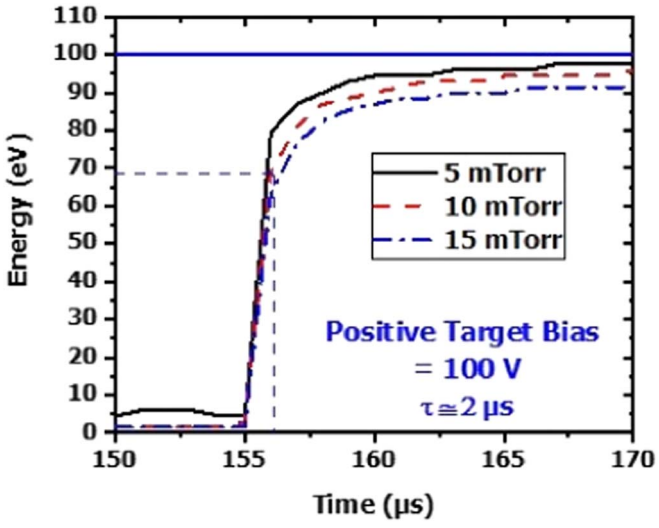

Figure 5. Visualization of transit time calculation. Kick pulse turns on at 154 μs, IEDF maximum energy reaches 67 V (67% of 100 V) at 156 μs. Discharge conditions: Pressures = 0.67 Pa (5 mTorr), 1.33 Pa (10 mTorr) and 2.00 Pa (15 mTorr) with a positive target bias width of 100 μs.

measurement of the plasma potential as a function of time shows the same effects [33]. The dip observed at the end of the 0.67 Pa case is caused by the power supply being unable to sustain the 100 V positive kick voltage for the entire duration of the kick, which is sometimes observed at the end of long kick pulses at low pressure. This phenomenon is also seen in figure 3(a).

3.3. Ion energy distributions

Figure 3 showcases the IEDF for a HiPIMS discharge of 150 μs main pulse with a 100 μs kick pulse with a 100 V positive target voltage for three different pressures. These surface plots clearly show the evolution of the IEDF, showcasing the rise in energy during the kick pulse. The major differences across pressure are mostly visible

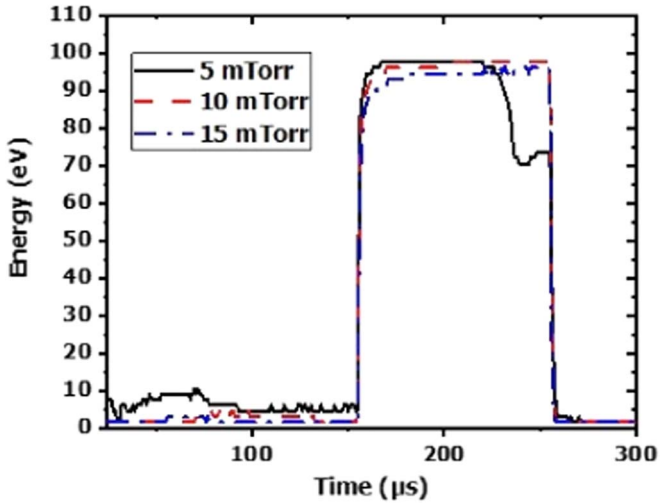

Figure 6. Energy of peak intensities of IEDF. Discharge condition: Kick voltage = 100 V, begins at 154 μs, with a main pulse length of 150 μs, kick pulse length of 100 μs at pressures of 0.67 Pa (5 mTorr), 1.33 Pa (10 mTorr), and 2.00 Pa (15 mTorr).

during the main pulse, as collisionality will lead to a decrease in mean energy. However, these waterfall plots by themselves convey too much information and are therefore broken down into different figures to try and understand and compare the three cases. A more concrete view is shown in figure 4 which examines 2D slices in time of the distribution function. The ion energy distribution during the main pulse (70 and 140 μs in figure 4) is shifted to lower peak energies as the pressure increases. Figure 4 also shows the HiPIMS I-V traces taken with floating probe data to show the methodology for comparison. The shots are all taken when rarefaction happens as the authors believe that is the best way to draw comparisons across pressure. This is expected due to the increased collisionality. At 0.67 Pa, the energy of the ions reaching the substrate is like the expected distribution which is a partially thermalized Maxwellian [39].

Complimentary to the peak energy of the IEDF, the width of the distribution is of critical importance to material processing applications looking to make use of tailored ion energies. While the RFEA technique used in this study is not capable of distinguishing low populations of multi-ionized species at high energy due to detector noise, understanding the variability of the full width at half maximum (FWHM) for the rest of the IEDF will guide the HiPIMS user in selecting conditions provided they remain below a current density likely to produce hot spots [3] or other magnetron instabilities.

To characterize the energy distribution reaching the substrate during the kick pulse FWHM was easily calculated as the peak shape is reasonably symmetric, notable exceptions to this being early in the kick pulse; this 'early' kick behaviour will be discussed later. FWHM values during the main pulse are inherently more inaccurate given the asymmetry of the distribution, as the distribution is Maxwellian, and not symmetric as it is observed to be during the positive cathode reversal. The method for calculating the FWHM was by finding the width of the distribution where the intensity drops to half, instead of fitting the dataset. This approximation was made due to the changing profile of the distribution and was intended to approximate the widths. As shown in figure 7, the FWHM does not vary significantly during the kick pulse regardless of conditions used. Figure 7(a) shows the pressure dependence of energy broadening during the entirety of the pulse. The dashed line indicates the beginning of the kick pulse, which occurs at 150 μs. For the three pressures (0.67 Pa, 1.33 Pa, and 2.00 Pa) the broadening during the main pulse is different, however after the positive cathode reversal is engaged the FWHM of the peaks drops significantly and is consistent across a wide pressure range. This highlights the energy control of the positive cathode reversal, and may allow for energetic deposition at higher pressures, which typically was hindered by increased collisionality at higher pressures. This is further evidence that the main acceleration mechanism of ion energy to the substrate is the sheath drop at the substrate itself. Additionally, when comparing the kick pulse length as shown in figure 7(b), the behaviour of the broadening is the same. This suggests that the physics at play here is independent of the length of the pulse and more so dependent on the conditions before the positive cathode reversal.

Figure 8 shows the variation of the IEDF at 0.67 Pa, 40 V kick pulse height and a 150 μs main pulse as a function of positive pulse length (25, 50 and 100 μs). During the positive cathode reversal the energy stays at the same value. Once pulse has ended, the ion energy drops back to its main-pulse values. One interesting note is the IEDF at 250 μs for the 100 μs kick pulse case. This IEDF is taken right as the positive pulse is turned off, and the energy is dropping to an intermediate form as the potential dies away. A few microseconds later, the IEDF again

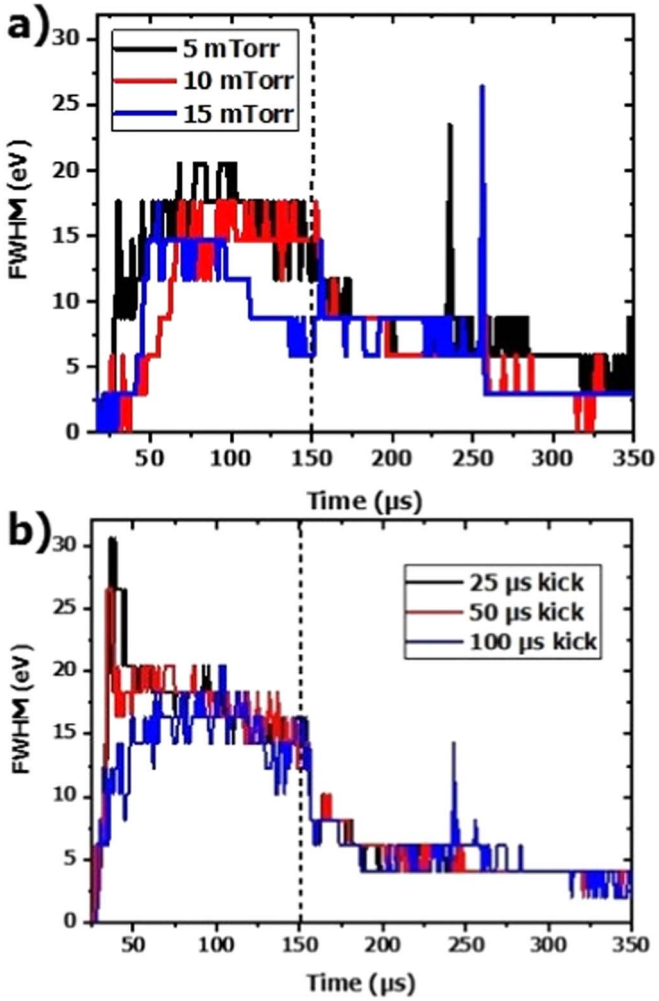

Figure 7. (a) FWHM plots for conditions of 150 μs main pulse, 100 μs kick pulse with a kick pulse positive voltage of 100 V, at pressures of 0.67 Pa (5 mTorr), 1.33 Pa (10 mTorr), and 2.00 Pa (15 mTorr). (b) FWHM varying kick pulse lengths at constant 1.33 Pa pressure and 40 V positive target voltage. Vertical dashed black line marks the start of the kick pulse and is intended as a guide to the eye only.

overlaps with the shorter positive pulse cases. A similar drop in plasma density is seen in the afterglow regions in figure 3 and tracks with the accelerated drop in plasma density with a positive pulse observed in Langmuir probe measurements by others [29]. Figure 8 was constructed so that the last trace was 50 μs after the end of the positive pulse, for this reason the runs with shorter positive pulses have fewer traces displayed. A recent article has also demonstrated that when the positive pulse length is increased the percentage of high energy ions, for both working gas and sputtered material increases [22]. This may appear to contradict the results presented here, but this work is time resolved, and if the average energy was presented it has been observed to follow the same trend. While the individual slices in time may appear identical, the positive pulse staying on will increase the total number of ions arriving with increased energy when the entire waveforms are time averaged.

3.4. Early kick

Of particularly interest is the higher FWHM of the kick pulse in the first ~20 μs after the main pulse ends, as shown in figure 7(b) for all kick pulse lengths. This broadening of the IEDF, relative to the remainder of the kick pulse, is similarly visible in the region of figure 3 annotated 'early kick', which is visible as a high energy tail, as well is in figure 4 comparing the 160 and 200 μs slices. This feature is persistent for all three pressures as shown in figures 3, 4 and 7(a). The feature must be properly explained in order to fully understand the transient evolution of the plasma and specifically the IEDF present in a deposition chamber as the kick pulse begins. Implications of this understanding are also critical to enabling HiPIMS to deliver tailored ion energies to materials process applications as this region offers the least control over the width of the IEDF. The understanding of the authors is that the early kick pulse is in part the product of a distinct process from the reminder of the kick pulse as explained below.

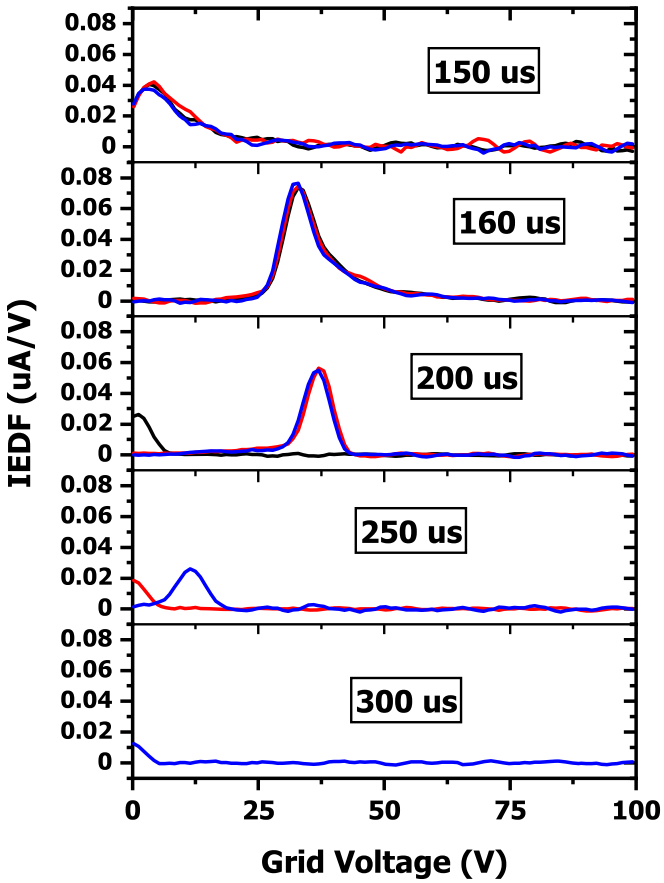

Figure 8. IEDF Time slices for 25 μs (black), 50 μs (red), and 100 μs (blue) kick pulse durations. Discharge conditions: Pressure = 0.67 Pa, main pulse = 150 μs, positive target voltage = 40 V.

When the main pulse ends and the positive target bias begins, the dense and highly ionized plasma in the magnetic trap is expelled to fill the volume of the chamber. We learned from measurements of transit times, as well as from approximated ambipolar diffusion calculations and from more in depth ambipolar diffusion calculations from literature [38], that this process is not instantaneous. Additionally, measurements of V_p have also shown a similar transit time [23], and measured EEDF show the presence of fast electrons at the start of the positive cathode reversal that are believed to cause the increase in V_p [23]. In the interim period, the plasma already in the chamber is partially ionized from the main pulse. The ions that are present pre-expansion bear an IEDF most similar to that of the last few μs of the main pulse, i.e.: broadly distributed, but at energies $<$20 eV. These ions, upon experiencing a shift to a positive plasma potential, are accelerated away from the target with additional energy as described by the pseudo-Hall thruster mechanism, meaning existing ions that are farther from the magnetic trap are accelerated by the polarity change on the target. The additional energy is substantially lower ($\sim$50%) than the applied kick bias, though this may be attributed to gas collisions *en route* to the probe. In this early part of the kick, the sheath present on the probe has not yet responded to the shift to positive plasma potential; rather it is expected to be of similar magnitude as during the main pulse. This shift in energy can be observed in figure 9 as the IEDF from just after the main pulse is shifted to higher energy by the kick bias. The IEDF at 58 and 60 μs for the 0.67 Pa case are very similar in shape apart from the shift in voltage while the higher-pressure cases likewise retain the shape but with greater intensity loss, which we believe could be caused by transport or by small differences in discharge conditions as the max intensity in the main pulse for cases a, b, and c are also different.

By 70 μs in figure 9, the ions present in the chamber outside the magnetic trap have all been accelerated to a grounded surface and the IEDF narrows to the distribution present for the remainder of the kick pulse, across all pressures. This distribution is the result of the plasma potential commuting across the chamber, as well as potentially enroute ionization caused by the plasma expansion. The expanding plasma likewise forms a transient sheath at the surface of the probe or at a substrate. The ions formed by the plasma expansion fall through this sheath and are accelerated to form the IEDF seen longer into the kick pulse without the high energy tail. The lifetime of this tail was not affected by the overall length of the kick pulse reaffirming that the tail is the result of a separate phenomenon. While we have not measured the species of the arriving ions on the substrate, we expect

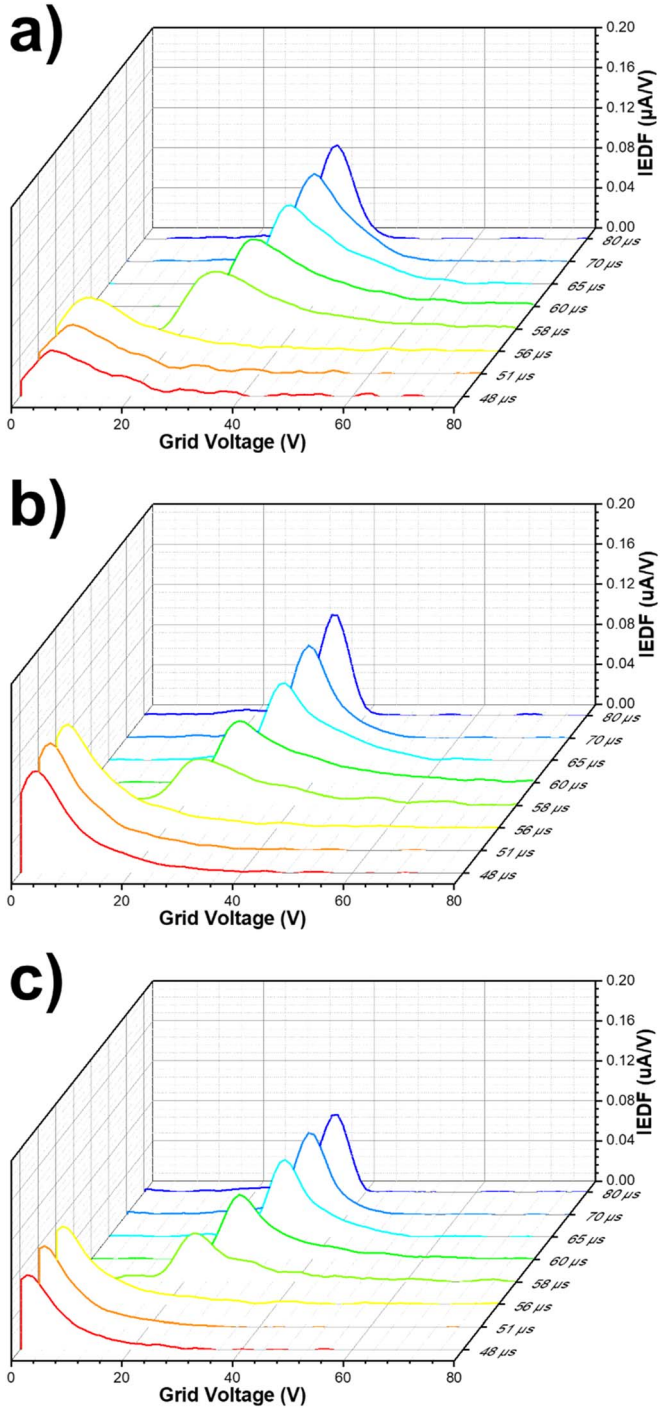

Figure 9. Waterfall plot of main to kick pulse transition. Main pulse is the first 50 μs then the kick pulse is on for the next 30 μs after a 4 μs delay, Kick pulse positive voltage of 40 V. Pressures are (a) 0.67 Pa, (b) 1.33 Pa, and (c) 2.00 Pa.

that the first group to arrive at 60 μs are most likely to be predominantly target ions and the ones near the end of the kick pulse are most likely to be predominantly Ar, the process gas. This theory is best supported by Viloan *et al* who examine the Ti and Ar high energy fractions for various positive kick pulse lengths [22]. They find that for shorter positive pulse lengths the high energy Ti^+ fraction is drastically higher, whereas after around a 400 μs positive pulse that the ratio is roughly 50-50 [22].

3.5. Total ion flux

Beyond the control of the IEDF to tailor ion energy, one of the longest running drawbacks to HiPIMS is reduced deposition rates compared to dcMS, primarily due to return of ionized material in the sheath to the target [8]. There has already been an effort to mitigate this through lowering the main pulse duration even without a kick pulse [9]. In the course of investigating the shape of the IEDF, integrations of the IEDF were likewise produced in

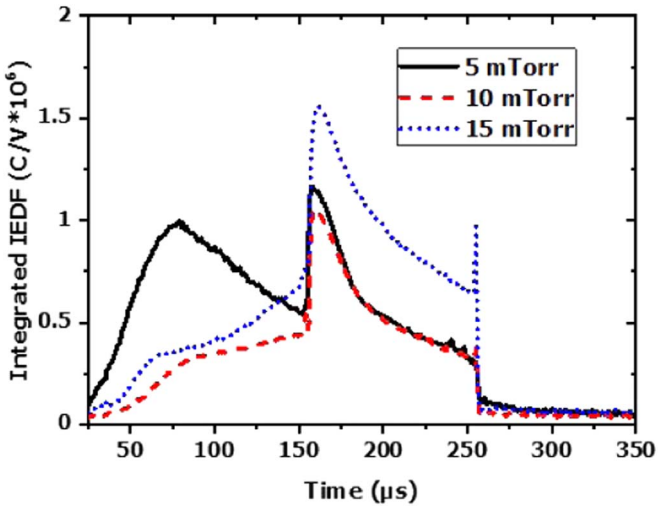

Figure 10. Integrated IEDF at varying pressure. *Y*-axis bears units of (current/bias * time), intended to represent net ion flux. Discharge conditions: main pulse = 150 μs, kick pulse = 100 μs, kick pulse positive voltage = 60 V.

order to determine relative total ion flux. As neutral metal deposition rates were not recorded, along with a differentiation between process gas and metal ions [1], the integrated IEDF cannot be used as a measure of total deposition rate. Nonetheless, figure 10 offers some insight into the ability of HiPIMS to produce heavily ionized deposition processes given the nearly doubling of ion flux during the kick pulse at higher pressures. In figure 10, the voltage was tuned such that the rarefaction would occur, however in the 0.67 Pa case the current sharply declines, and in the 1.33 Pa case the current also decreases slightly after rarefaction. However, after the current rolls over in the 2.00 Pa case the current holds a constant value. This may explain why the 2.00 Pa case has significantly higher ion flux during the kick as the discharge is able to hold its peak current. Ultimately, complimentary techniques such as time-resolved mass spectroscopy, will need to be performed in tandem with IEDF measurements to ascertain if gains in ion flux are dominated by process gas or metal species as this technique cannot determine ionization fraction.

4. Conclusions

The time-resolved ion energy distribution function for a HiPIMS discharge with a kick pulse has been systematically studied over stable process conditions. Most significantly, the observation of a high energy tail to the IEDF early in the kick, followed by a more symmetric distribution, suggests a transition from a pseudo-Hall thruster like acceleration of ions, or the acceleration of ions that are not near the magnetic trap, to ions falling in potential from V_p to a grounded surface after the plasma potential commutes throughout the chamber. The transit time of the plasma, the IEDF width, and peak energy were all found to be weakly dependent on pressure suggesting that process intensification may be possible with higher deposition rates while retaining the precise ion energy control that HiPIMS offers. Only the early kick appears to have dependence on pressure which strengthens the argument that the high energy tail found early in the positive pulse is metal ions being accelerated by a pseudo-Hall thruster as transport losses would lead to lower mean energy during the main pulse with fewer ions at higher energies. It has been demonstrated that the kick pulse energy commutes to the probe within 2–4 μs regardless of conditions, and that the IEDF width during the kick is on the order of 5 eV which for most cases is less broad than during the main pulse.

Acknowledgments

The work in this publication was funded by the Department of Energy award DE-SC0020689. The authors wish to thank the application support at Impedans for many helpful conversations regarding probe operation and optimization.

Data availability statement

All data that support the findings of this study are included within the article (and any supplementary files).

ORCID iDs

David E Barlaz https://orcid.org/0000-0001-8915-2059
David N Ruzic https://orcid.org/0000-0001-9501-1439

References

[1] Keraudy J, Viloan R P B, Raadu M A, Brenning N, Lundin D and Helmersson U 2019 Bipolar HiPIMS for tailoring ion energies in thin film deposition *Surf. Coat. Technol.* **359** 433–7
[2] Alami J, Sarakinos K, Mark G and Wuttig M 2006 On the deposition rate in a high power pulsed magnetron sputtering discharge *Appl. Phys. Lett.* **89** 154104
[3] Raman P, Cheng M, Weberski J, Xu W, Houlahan T, Rivera J, Su R, Shchelkanov I and Ruzic D 2018 Magnetic field influence on ionization zones in high-power impulse magnetron sputtering *Vacuum* **156** 9–19
[4] Gudmundsson J T, Brenning N, Lundin D and Helmersson U 2012 High power impulse magnetron sputtering discharge *Journal of Vacuum Science & Technology A* **30** 030801
[5] McLain J, Raman P, Patel D, Spreadbury R, Uhlig J, Shchelkanov I and Ruzic D N 2018 Linear magnetron HiPIMS high deposition rate magnet pack *Vacuum* **155** 559–65
[6] Raman P, Shchelkanov I, McLain J, Cheng M, Ruzic D, Haehnlein I, Jurczyk B, Stubbers R and Armstrong S 2016 High deposition rate symmetric magnet pack for high power pulsed magnetron sputtering *Surf. Coat. Technol.* **293** 10–5
[7] Raman P, Weberski J, Cheng M, Shchelkanov I and Ruzic D N 2016 A high power impulse magnetron sputtering model to explain high deposition rate magnetic field configurations *J. Appl. Phys.* **120** 163301
[8] Christie D J 2005 Target material pathways model for high power pulsed magnetron sputtering *Journal of Vacuum Science & Technology A* **23** 330–5
[9] Shimizu T, Zanáška M, Villoan R, GBrenning N, Helmersson U and Lundin D 2021 Experimental verification of deposition rate increase, with maintained high ionized flux fraction, by shortening the HiPIMS pulse *Plasma Sources Sci. Technol.* **30** 045006
[10] Ehiasarian A P 2010 High-power impulse magnetron sputtering and its applications *Pure Appl. Chem.* **82** 1247–58
[11] Bohlmark J, Lattemann M, Gudmundsson J T, Ehiasarian A P, Aranda Gonzalvo Y, Brenning N and Helmersson U 2006 The ion energy distributions and ion flux composition from a high power impulse magnetron sputtering discharge *Thin Solid Films* **515** 1522–6
[12] Ehiasarian A P, New R, Münz W D, Hultman L, Helmersson U and Kouznetsov V 2002 Influence of high power densities on the composition of pulsed magnetron plasmas *Vacuum* **65** 147–54
[13] Anders A, Andersson J and Ehiasarian A 2007 High power impulse magnetron sputtering: current-voltage-time characteristics indicate the onset of sustained self-sputtering *J. Appl. Phys.* **102** 113303
[14] Meng L, Yu H, Szott M M, McLain J T and Ruzic D N 2014 Downstream plasma transport and metal ionization in a high-powered pulsed-plasma magnetron *J. Appl. Phys.* **115** 223301
[15] Meng L, Yu H, Sporre J R, Raman P, Szott M M, McLain J T and Ruzic D N 2015 Direct measurement and modeling of the redirected ion flux in a high-powered pulsed-plasma magnetron *Journal of Vacuum Science & Technology A* **33** 031301
[16] Anders A 2010 Deposition rates of high power impulse magnetron sputtering: physics and economics *Journal of Vacuum Science & Technology A* **28** 783–90
[17] Green K M, Hayden D B, Juliano D R and Ruzic D N 1997 Determination of flux ionization fraction using a quartz crystal microbalance and a gridded energy analyzer in an ionized magnetron sputtering system *Rev. Sci. Instrum.* **68** 4555–60
[18] Juliano D R, Ruzic D N, Allain M M C and Hayden D B 2002 Influences on ionization fraction in an inductively coupled ionized physical vapor deposition device plasma *J. Appl. Phys.* **91** 605–12
[19] Wu B, Haehnlein I, Shchelkanov I, McLain J, Patel D, Uhlig J, Jurczyk B, Leng Y and Ruzic D N 2018 Cu films prepared by bipolar pulsed high power impulse magnetron sputtering *Vacuum* **150** 216–21
[20] Konstantinidis S, Dauchot J P, Ganciu M, Ricard A and Hecq M 2006 Influence of pulse duration on the plasma characteristics in high-power pulsed magnetron discharges *J. Appl. Phys.* **99** 013307
[21] Ruzic D N, Stubbers R A and Jurczyk B E 2018 Pulsed power module with pulse and ion flux control for magnetron sputtering US20180358213A1 https://patents.google.com/patent/US20180358213A1/en?oq=US20180358213A1
[22] Viloan R P B, Zanáška M, Lundin D and Helmersson U 2020 Pulse length selection for optimizing the accelerated ion flux fraction of a bipolar HiPIMS discharge *Plasma Sources Sci. Technol.* **29** 125013
[23] Hippler R, Cada M and Hubicka Z 2021 A positively biased external anode for energy control of plasma ions: hollow cathode and magnetron sputtering discharge *Plasma Sources Sci. Technol.* **30** 045003
[24] Pajdarová A D, Kozák T, Hubička Z, Čada M, Mareš P and Čapek J 2020 Plasma parameters in positive voltage pulses of bipolar HiPIMS discharge determined by Langmuir probe with a sub-microsecond time resolution *Plasma Sources Sci. Technol.* **29** 085016
[25] Anders A 2010 A structure zone diagram including plasma-based deposition and ion etching *Thin Solid Films* **518** 4087–90
[26] Velicu I-L, Ianoş G-T, Porosnicu C, Mihăilă I, Burducea I, Velea A, Cristea D, Munteanu D and Tiron V 2019 Energy-enhanced deposition of copper thin films by bipolar high power impulse magnetron sputtering *Surf. Coat. Technol.* **359** 97–107
[27] Hovsepian P E, Ehiasarian A P, Purandare Y P, Mayr P, Abstoss K G, Mosquera Feijoo M, Schulz W, Kranzmann A, Lasanta M I and Trujillo J P 2018 Novel HIPIMS deposited nanostructured CrN/NbN coatings for environmental protection of steam turbine components *J. Alloys Compd.* **746** 583–93
[28] Hovsepian P E, Ehiasarian A P, Purandare Y P, Braun R and Ross I M 2009 Effect of high ion irradiation on the structure, properties and high temperature tribology of nanoscale CrAlYN/CrN multilayer coating deposited by HIPIMS-HIPIMS technique *Plasma Processes Polym.* **6** S118–23
[29] Hippler R, Cada M and Hubicka Z 2020 Time-resolved diagnostics of a bipolar HiPIMS discharge *J. Appl. Phys.* **127** 203303
[30] Britun N, Michiels M, Godfroid T and Snyders R 2018 Ion density evolution in a high-power sputtering discharge with bipolar pulsing *Appl. Phys. Lett.* **112** 234103
[31] Michiels M, Godfroid T, Snyders R and Britun N 2020 A poly-diagnostic study of bipolar high-power magnetron sputtering: role of electrical parameters *J. Phys. D: Appl. Phys.* **53** 435205
[32] Zhou G, Wang L, Wang X and Yu Y 2020 Investigating the plasma parameters and discharge asymmetry in dual magnetron reactive high power impulse magnetron sputtering discharge with Al in Ar/O_2 mixture *Vacuum* **175** 109253

[33] Huber W, Houlahan T, Jeckell Z, Barlaz D, Jurczyk B and Ruzic D 2022 Time resolved electron energy distribution functions during a HiPIMS discharge *Plasma Sources Sci. Technol.* **31** 065001
[34] Huo C, Raadu M A, Lundin D, Gudmundsson J T, Anders A and Brenning N 2012 Gas rarefaction and the time evolution of long high-power impulse magnetron sputtering pulses *Plasma Sources Sci. Technol.* **21** 045004
[35] Maszl C, Breilmann W, Benedikt J and von Keudell A 2014 Origin of the energetic ions at the substrate generated during high power pulsed magnetron sputtering of titanium *J. Phys. D: Appl. Phys.* **47** 224002
[36] Meng L, Cloud A N, Jung S and Ruzic D N 2011 Study of plasma dynamics in a modulated pulsed power magnetron discharge using a time-resolved Langmuir probe *Journal of Vacuum Science & Technology* A **29** 011024
[37] Wu Y L, Hong J, Ouyang Z, Cho T S and Ruzic D N 2013 Electrical and optical characteristics of cylindrical non-thermal atmospheric-pressure dielectric barrier discharge plasma sources *Surf. Coat. Technol.* **234** 100–3
[38] Han M, Luo Y, Li L, Gu J, Xu Y and Luo S 2021 Optimizing the ion diffusion in bipolar-pulse HiPIMS discharge (BP-HiPIMS) via an auxiliary anode *Plasma Sources Sci. Technol.* **30** 095016
[39] Held J, Thiemann-Monjé S, von Keudell A and Schulz-von der Gathen V 2020 Velocity distribution of metal ions in the target region of HiPIMS: the role of Coulomb collisions *Plasma Sources Sci. Technol.* **29** 125003